

R²Energy: A Large-Scale Benchmark for Robust Renewable Energy Forecasting under Diverse and Extreme Conditions

Zhi Sheng¹, Yuan Yuan², Guozhen Zhang³, Yong Li¹

¹Center for Urban Science and Computation, Tsinghua University

²Courant Institute of Mathematical Sciences, New York University

³TsingRoc.ai

Abstract

The rapid expansion of renewable energy, particularly wind and solar power, has made reliable forecasting critical for power system operations. While recent deep learning models have achieved strong average accuracy, the increasing frequency and intensity of climate-driven extreme weather events pose severe threats to grid stability and operational security. Consequently, developing robust forecasting models that can withstand volatile conditions has become a paramount challenge. In this paper, we present R²Energy, a large-scale benchmark for NWP-assisted renewable energy forecasting. It comprises over 10.7 million high-fidelity hourly records from 902 wind and solar stations across four provinces in China, providing the diverse meteorological conditions necessary to capture the wide-ranging variability of renewable generation. We further establish a standardized, leakage-free forecasting paradigm that grants all models identical access to future Numerical Weather Prediction (NWP) signals, enabling fair and reproducible comparison across state-of-the-art representative forecasting architectures. Beyond aggregate accuracy, we incorporate regime-wise evaluation with expert-aligned extreme weather annotations, uncovering a critical “robustness gap” typically obscured by average metrics. This gap reveals a stark robustness-complexity trade-off: under extreme conditions, a model’s reliability is driven by its meteorological integration strategy rather than its architectural complexity. R²Energy provides a principled foundation for evaluating and developing forecasting models for safety-critical power system applications.

1 Introduction

The global imperative for carbon neutrality has accelerated the deployment of renewable energy sources, particularly wind and solar photovoltaic (PV) power [12, 15, 42, 46, 48]. In China, the “Dual Carbon” goals, aiming for Carbon Peaking by 2030 and Carbon Neutrality by 2060, have driven installed capacity to unprecedented levels [34, 49]. However, the inherent intermittency and volatility of renewable energy increasingly jeopardize power system stability as penetration rises [38, 44–46, 48]. Consequently, modern grid operations, such as unit commitment and dispatch, now rely on accurate, look-ahead forecasting [4, 20, 39], necessitating a paradigm shift from classical time-series extrapolation to Numerical Weather Prediction (NWP)-assisted, cross-domain modeling [5, 18, 20, 40].

Meanwhile, climate change introduces a critical paradox: the energy sources designed to mitigate climate risks are themselves highly sensitive to intensifying weather variability [14, 38, 45, 48]. As extreme events such as torrential rainstorms and prolonged heatwaves become the “new normal,” power systems face heightened operational stress [14, 45, 48]. In these regimes, grid stability depends not on average-case accuracy, but on a model’s ability to

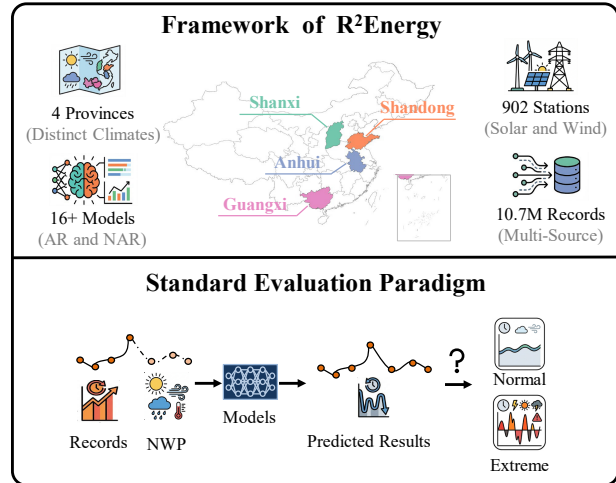


Figure 1: Overall framework of R²Energy.

anticipate abrupt ramp-downs and efficiency losses. Developing NWP-informed forecasting frameworks that remain robust under these extreme conditions is therefore essential for reliable resource allocation and the security of safety-critical power systems [45, 48].

Despite the rapid proliferation of deep learning architectures [13, 29, 35], ranging from RNNs [28] and Transformers [5, 33] to advanced MLPs [25, 43] and generative models [8, 41], the academic community continues to evaluate renewable energy forecasting primarily through aggregated metrics like Mean Absolute Error (MAE) [5, 17, 18, 39]. This average-case evaluation paradigm obscures a critical vulnerability: model fragility under extreme meteorological conditions. A forecasting system that achieves a marginal reduction in overall error yet fails catastrophically during an abrupt storm front or extreme heat event poses substantial risks to power grid security and operational reliability [10, 22, 26, 27]. Two fundamental obstacles hinder progress: (i) the reliance on isolated, limited datasets that lack diverse climatic regimes, and (ii) the absence of standardized protocols for incorporating future NWP signals, which leads to inherently unfair comparisons between autoregressive and non-Autoregressive models. Consequently, current benchmarks fail to distinguish models that are “good on average” from those that remain reliable under the high-impact, low-frequency events critical for safety-critical power grid operations [1, 21, 23, 30, 39]. There is an urgent need for a benchmark that moves beyond aggregate statistics to rigorously evaluate forecasting reliability across heterogeneous climatic regions and meteorological extremities.

To bridge the robustness-evaluation gap identified above, we present **R²Energy** (benchmark for **R**obust **R**newable **E**nergy forecasting). This large-scale, multi-source benchmark evaluates forecasting reliability across two orthogonal dimensions: climatic diversity across distinct geographical regions and meteorological extremity during critical weather events. Moving beyond simple time-series extrapolation, R²Energy redefines renewable forecasting as an NWP-assisted mapping process. Formally, the task learns the mapping $(X, C) \rightarrow \hat{y}$ within a standardized, leakage-free protocol that ensures all models have identical access to future exogenous signals, enabling fair and reproducible “stress testing”. Crucially, to address model reliability under stress, we move beyond aggregate error metrics by introducing the Qualification Rate (Q) to measure industrial safety compliance.

As shown in Figure 1, built upon 10.7 million high-fidelity hourly records from 902 wind and solar stations across four diverse climatic regions in China (Anhui, Shanxi, Shandong, and Guangxi), R²Energy provides the unprecedented scale required to evaluate models against high-impact, tail-risk events. By benchmarking 16 state-of-the-art models through a regime-wise lens, we uncover a critical robustness-complexity trade-off typically obscured by previous studies [39, 43]: performance is driven less by architectural complexity than by a model’s meteorological integration strategy. Empirically, Autoregressive models, specifically GRU, prove remarkably stable, as their dynamic injection of future NWP signals effectively anchors recursive trajectories and mitigates classical error accumulation. Conversely, Transformer variants exhibit heightened sensitivity and instability in noisy regimes, such as volatile wind fields. These findings highlight why protocol-aligned robustness is non-negotiable for the deployment of safety-critical power systems. Our contributions are summarized as follows:

- We present R²Energy, a massive benchmark comprising 10.7M records from 902 stations. We leverage this scale to evaluate 16 state-of-the-art models under diverse operational conditions.
- We establish a standardized, leakage-free forecasting protocol that redefines renewable forecasting as an NWP-assisted mapping task. Beyond standard error metrics, we introduce the Qualification Rate (Q) for industrial safety compliance.
- We propose a regime-wise, extreme-aware evaluation paradigm using expert-aligned weather annotations that rigorously assess model reliability under non-linear distribution shifts and high-impact tail risks.
- Our analysis uncovers a critical robustness-complexity trade-off, revealing that a model’s reliability under pressure is primarily driven by its meteorological integration strategy rather than its architectural complexity.

2 Preliminaries

In this section, we define the notation and the problem formulation for the NWP-assisted renewable energy forecasting task. We denote scalars in normal font (e.g., y), vectors in bold lowercase (e.g., \mathbf{x}), and tensors/sets in calligraphic or capital bold font (e.g., \mathcal{D}, \mathbf{X}).

Data Representation. We consider a dataset $\mathcal{D} = \{\mathbf{S}^{(i)}\}_{i=1}^{N_{\text{station}}}$ collected from N_{station} renewable energy stations. At time t , the

system state of station i is described by the capacity factor

$$y_t^{(i)} = \frac{P_{\text{out},t}^{(i)}}{P_{\text{rated}}^{(i)}} \in [0, 1], \quad (1)$$

together with historical covariates $\mathbf{x}_t^{(i)} \in \mathbb{R}^{d_x}$ and a future context vector $\mathbf{c}_t^{(i)} \in \mathbb{R}^{d_c}$ derived from NWP forecasts and deterministic temporal features, which are known *a priori* for the forecasting horizon. Data quality is indicated by a binary mask $M_t^{(i)} \in \{0, 1\}$, where $M_t^{(i)} = 1$ denotes missing or anomalous observations.

Sample Construction. Using a sliding window with history length L and forecasting horizon H , we construct samples $\xi_k^{(i)} = (\mathbf{X}_k^{(i)}, \mathbf{C}_k^{(i)}, \mathbf{Y}_k^{(i)})$, where

$$\mathbf{X}_k^{(i)} = [(y_t^{(i)}, \mathbf{x}_t^{(i)})]_{t=t_k-L+1}^{t_k} \in \mathbb{R}^{L \times (1+d_x)}, \quad (2)$$

$$\mathbf{C}_k^{(i)} = [\mathbf{c}_t^{(i)}]_{t=t_k+1}^{t_k+H} \in \mathbb{R}^{H \times d_c}, \quad (3)$$

$$\mathbf{Y}_k^{(i)} = [y_t^{(i)}]_{t=t_k+1}^{t_k+H} \in \mathbb{R}^{H \times 1}. \quad (4)$$

To ensure the benchmark evaluates forecasting performance rather than imputation, a sample is retained only if all involved time steps are valid:

$$\sum_{t=t_k-L+1}^{t_k+H} M_t^{(i)} = 0. \quad (5)$$

NWP-Assisted power Forecasting. Given a historical observation tensor $\mathbf{X} \in \mathbb{R}^{L \times (1+d_x)}$ and the future exogenous context $\mathbf{C} \in \mathbb{R}^{H \times d_c}$ derived from NWP forecasts, the goal is to predict the future capacity factor trajectory $\mathbf{Y} \in \mathbb{R}^{H \times 1}$ over a horizon H . We employ a parametric model f_θ to approximate the mapping $\hat{\mathbf{Y}} = f_\theta(\mathbf{X}, \mathbf{C})$. The optimal parameter set θ^* is determined by minimizing the expected discrepancy between the predicted and ground-truth trajectories over the valid sample space Ω_{valid} :

$$\theta^* = \arg \min_{\theta} \mathbb{E}_{(\mathbf{X}, \mathbf{C}, \mathbf{Y}) \in \Omega_{\text{valid}}} [\ell(f_\theta(\mathbf{X}, \mathbf{C}), \mathbf{Y})]. \quad (6)$$

3 The R²Energy Framework

Reliable evaluation of renewable energy forecasting models hinges on both the scale of available data and the diversity of underlying physical regimes. In this section, we introduce **R²Energy**, a large-scale, multi-source benchmark designed to capture the heterogeneity of real-world renewable generation across space, time, and extreme operating conditions.

3.1 Dataset Overview

In this section, we introduce the R²Energy dataset in detail and analyze the characteristics of different datasets as well as the impacts of extreme weather events.

Renewable Energy Station Data. We have constructed a massive multi-source dataset comprising over 10.7 million hourly records, covering both wind and solar power generation across four distinct climatic regions in China: Anhui, Shanxi, Shandong, and Guangxi. As detailed in Table 1, this dataset includes 902 individual stations, offering a high degree of geographic diversity and scale compared to previous benchmarks. To standardize the prediction target across

Table 1: Statistics of the six datasets. The rightmost column lists the variables and settings shared by all datasets.

Type	Dataset	Province	# of Stations	Time Period	Total Records	Extreme (Lvl 1-3)		Variables & Settings
						Rainstorm	Heatwave	
Wind	W1	Anhui	110	2023-01-01 – 2024-11-18	1,548,258	6,723	56,839	Physical Vars: $ws_{10}, ssrd, u_{10}, v_{10}, t_{2m}, tp, CF$ Quality Control: Masks for Missing & Outliers
	W2	Shanxi	233	2023-10-30 – 2025-03-25	2,324,213	1,882	3,953	
	W3	Shandong	20	2024-12-01 – 2025-07-14	82,752	0	2,164	
Solar	S1	Anhui	242	2023-01-01 – 2024-11-18	3,545,797	13,771	135,802	Extreme Labels: Rainstorm & Heatwave (Lvl 1-3)
	S2	Shanxi	241	2023-10-30 – 2024-12-31	2,362,101	2,434	7,848	
	S3	Guangxi	56	2023-01-01 – 2025-01-01	902,917	899	978	

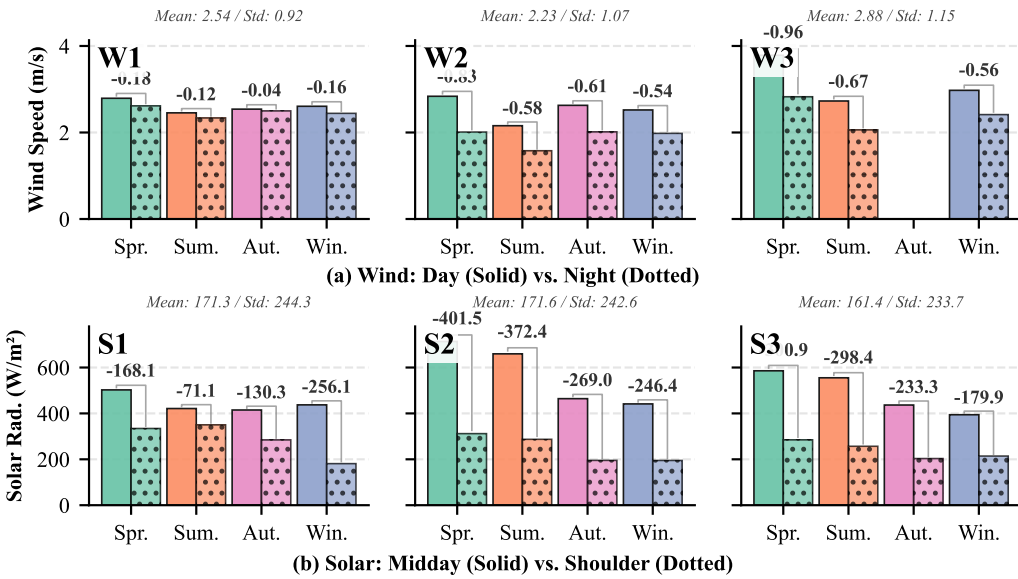


Figure 2: Intra-day and seasonal variability across the wind and solar datasets. The top row (a) illustrates the average wind speed (m/s) variations between daytime (07:00–18:00, solid bars) and nighttime (dotted bars). The bottom row (b) compares solar radiation (W/m^2) during peak midday hours (11:00–14:00, solid bars) versus shoulder hours (morning/evening, dotted bars). The numerical labels above the brackets denote the difference between the two periods, while the global mean and standard deviation are listed for each dataset. Missing bars in W3 indicate data unavailability for specific seasons.

stations with varying capacities—and to account for dynamic capacity changes due to potential expansion—we utilize the *Capacity Factor* (CF) as the ground truth. The CF is calculated by dividing the raw power output by the real-time rated capacity of the station.

Meteorological Data. Reliable meteorological information is critical for mapping weather conditions to power output. We utilize the ERA5-Land reanalysis dataset [31], which offers a high spatial resolution of 0.1° and an hourly temporal resolution. We acquire site-specific meteorological conditions for each station via bilinear interpolation. In this benchmark, these ERA5 variables serve a dual purpose: they act as historical covariates and, crucially, as a high-fidelity proxy for future *Numerical Weather Prediction* (NWP) signals. While operational NWP forecasts contain inherent errors, using reanalysis data as a "perfect prognosis" proxy isolates the forecasting model's mapping capability from the noise of weather prediction errors. This allows us to rigorously evaluate whether

a model can effectively learn the physical relationship between weather and power generation.

Distribution Characteristics. To explicitly characterize the distribution diversity of the target variables, we analyzed the spatiotemporal patterns of Wind Speed and Solar Radiation, the primary meteorological drivers of power generation. As illustrated in Figure 2, the datasets exhibit distinct distributional shifts across different climatic zones. The wind datasets cover a spectrum from stable to highly volatile regimes. As shown in Figure 2(a), W1 (Anhui) exhibits a "steady-state" characteristic with moderate wind speeds (~ 2.5 m/s) and minimal diurnal amplitude (day-night differences range only from -0.04 to -0.18 m/s). In stark contrast, W2 (Shanxi) and W3 (Shandong) represent "high-volatility" regimes typical of northern plains and coastal areas. Specifically, W3 demonstrates extreme diurnal fluctuations, with a sharp drop of -0.96 m/s during spring nights, while W2 maintains consistently high variability across all seasons (e.g., -0.61 m/s in autumn). This diversity

challenges forecasting models to adapt to both persistent patterns (W1) and rapid, high-amplitude transitions (W2/W3). Similarly, the solar datasets reveal significant differences in both intensity and seasonal phase. S2 (Shanxi) typifies a high-altitude, arid climate with intense radiation (Spring peak $> 600 \text{ W/m}^2$) and massive intra-day variability, evidenced by the steepest midday-to-shoulder drop of -401.5 W/m^2 . Conversely, S3 (Guangxi), located in a humid subtropical zone, shows a distinct seasonal phase shift (peaking in Summer rather than Spring) and significantly lower radiation variance during Spring ($+0.9 \text{ W/m}^2$ difference), likely attributed to the persistent cloud cover and rainfall characteristic of the southern rainy season. S1 (Anhui) serves as a transitional distribution with moderate intensity. R²Energy represents more than a mere expansion of data volume; it encompasses a comprehensive range of physical modalities. By covering diverse climatic regimes, our benchmark enables a more holistic evaluation of model generalization potential across varying physical constraints.

Extreme Weather Signals. To diagnose model reliability under stress, we annotate the timeline with extreme weather labels based on the official standards defined by the China Meteorological Administration (CMA). We focus on two high-impact categories: *Rainstorm* and *Heatwave*, each graded into three severity levels. Detailed information are shown in Table 2. To empirically validate the necessity of these annotations, we analyzed the power response characteristics under different meteorological states using the Shanxi (S2/W2) datasets. Figure 3 visualizes the aggregated diurnal curves for solar power and distributional box-plots for wind power during labeled Level 1-3 events versus normal periods. The results reveal profound physical divergences driven by extreme weather. In the solar domain (Figure 3a), rainstorms induce a drastic suppression effect, reducing the peak capacity factor to below 0.3—less than 50% of the normal baseline—due to thick cloud occlusion. Conversely, heatwaves coincide with high-irradiance clear-sky conditions, pushing the peak output above 0.75, significantly higher than the normal mean. In the wind domain (Figure 3b), we observe a clear regime-dependent distributional shift. Rainstorms, typically driven by convective systems, introduce stronger wind forcing and elevated turbulence, which shifts the operating distribution toward higher generation (median: $0.16 \rightarrow 0.27$), while heatwaves, often associated with stagnant high-pressure systems, lead to "wind droughts" with a reduced median of 0.10. These significant non-linear shifts confirm that extreme weather imposes distinct physical modalities on power generation. Consequently, forecasting models optimized solely for "average" conditions may fail catastrophically during these high-impact events. R²Energy addresses this critical gap by providing the precise annotations required to evaluate model robustness specifically under these tail-risk regimes.

3.2 Data Quality Control

Real-world operational data inevitably contains sensor failures and transmission anomalies. To ensure the benchmark evaluates physical modeling capability rather than data cleaning skills, we implement a strict quality-masking strategy. We generate a binary mask $M \in \{0, 1\}$ for the power series based on three rigorous criteria: (i) **Missing Values**: Any timestamp containing NaN values is immediately flagged. (ii) **Frozen Value Detection**: We identify

Table 2: Definition of extreme meteorological events and severity levels used in RexBench.

Event Type	Level	Warning	Criteria
Rainstorm	Level 1	Blue	Rainfall $\geq 50 \text{ mm}$ within 12 h
	Level 2	Yellow	Rainfall $\geq 50 \text{ mm}$ within 6 h
	Level 3	Orange	Rainfall $\geq 50 \text{ mm}$ within 3 h
Heatwave	Level 1	Yellow	Max temperature $> 35^\circ\text{C}$ for 3 consecutive days
	Level 2	Orange	Max temperature $> 37^\circ\text{C}$ within 24 h
	Level 3	Red	Max temperature $> 40^\circ\text{C}$ within 24 h

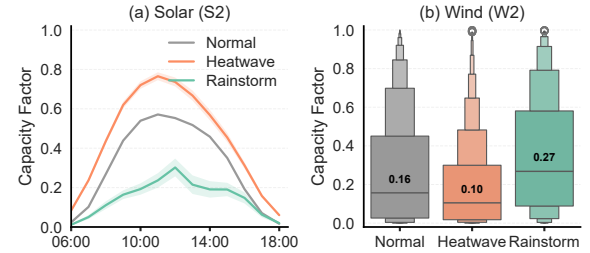


Figure 3: Impact of extreme weather on renewable power generation. (a) Solar (S2) and (b) Wind (W2) datasets. Shaded areas in (a) denote 95% confidence intervals; values in (b) indicate medians.

periods where the power output remains mathematically identical for more than 24 hours, which typically indicates sensor sticking or data logger failures. (iii) **Statistical Outlier Removal**: We calculate the Z-score of the power series. Data points deviating from the station's mean by more than a threshold $\theta = 3.0$ standard deviations are flagged as statistical anomalies. During the sample construction process, we adopt a "zero-tolerance" policy: any sample window containing even a single masked time step ($M = 1$) is strictly discarded. This approach differs from prior works that rely on interpolation, ensuring that our models are trained and evaluated solely on high-confidence, physically consistent observations.

3.3 Benchmarking Protocols

To ensure a fair and consistent comparison between diverse models, we standardize the injection mechanism for future NWP data, adapting the methodologies described in previous work [39].

Autoregressive (AR) Models. For AR models (e.g., LSTM [11], GRU [7]), which generate predictions iteratively, the NWP data is inserted dynamically at each future time step. Specifically, during the forecasting phase, the NWP vector c_t corresponding to the target timestamp is concatenated with the model's input (or hidden state) for that specific iteration. This simulates the operational availability of weather forecasts for each specific look-ahead hour.

Non-Autoregressive (NAR) Models. For NAR models, which predict the entire horizon simultaneously, the injection method depends on the specific architecture: (i) **General NAR Models (e.g., CNN/MLP-based)**: The future NWP sequence is typically treated as a known covariate channel. It is concatenated with the encoded hidden state vector or the input features, serving as a global condition for the decoder to generate the full sequence. (ii)

Table 3: Taxonomy of Renewable Energy Forecasting Horizons and Applications.

Forecast Type	Horizon	Operational Use Cases
Ultra-Short-Term (USTF)	≤ 1 hour	Real-time dispatch, Automatic Generation Control, Power Smoothing.
Short-Term (STF)	≤ 1 day	Economic Dispatch, Reserve Scheduling, Day-ahead Market Operations.
Medium-Term (MTF)	1–15 days	Unit Commitment, Maintenance Planning, Congestion Management.
Long-Term (LTF)	Months to years	Capacity Planning, Grid Expansion, Risk Assessment.

Transformer-based Models (e.g., Informer [47]): The NWP sequence is integrated into the generative inference process. The NWP data is zero-padded to match the dimensions of the decoder’s token input and then concatenated. This combined input is then processed through the embedding layers (Value, Position, and Temporal Embeddings) before being fed into the decoder, ensuring the attention mechanism can explicitly attend to future weather contexts.

4 Experimental Settings

In this section, we detail the experimental setup of R²Energy, including the task formulations, baseline models, evaluation metrics, and implementation protocols.

4.1 Operational Forecasting Regimes

In power system operations, renewable energy forecasting is categorized by standardized temporal horizons, each associated with distinct modeling assumptions and operational objectives [2, 19, 32]. Table 3 summarizes the commonly adopted forecasting regimes in the energy industry. R²Energy focuses on forecasting horizons within the USTF, STF, and MTF regimes, where future Numerical Weather Prediction (NWP) information is routinely available and operationally utilized. In all settings, historical observations $X_{t-L+1:t}$ and future NWP availability $C_{t+1:t+H}$ are utilized to predict the target $Y_{t+1:t+H}$: (i) **Ultra-Short-Term Forecasting (USTF):** Defined as using a historical window of $L = 24$ hours to predict the next $H = 1$ hour. (ii) **Short-Term Forecasting (STF):** Defined as using $L = 24$ hours of history to predict the next $H = 24$ hours (Day-Ahead). (iii) **Medium-Term Forecasting (MTF):** Defined as using $L = 72$ hours of history to predict the next $H = 72$ hours. This is critical for maintenance scheduling and congestion management.

4.2 Baseline Selection

To rigorously benchmark the proposed dataset, we evaluate a comprehensive suite of 16 representative models across three distinct categories: Statistical/Physical methods, Autoregressive (AR) models, and Non-Autoregressive (NAR) models.

Statistical and Physical Baselines. These methods serve as foundational benchmarks, representing physics-agnostic heuristics and domain-knowledge-driven estimations. **Seasonal-Naive:** Given the diurnal periodicity of renewable energy, we use the observation from the same timestamp of the previous day as the prediction: $\hat{y}_{t+h} = y_{t+h-24}$ (recursively applied for horizons $H > 24$). **Physics-Informed Models:** We implement classic physical conversion models [46] that map meteorological variables (subsets of the context vector c_t) to capacity factors. For **Solar Power**, let R_t be the solar irradiance (W/m^2) and T_t be the ambient air temperature ($^{\circ}C$) derived from c_t . The estimated capacity factor \hat{y}_t is calculated as:

$$\hat{y}_t = \frac{R_t}{R_{std}} \times [1 + \alpha_p(T_t - T_{std})], \quad (7)$$

where standard test conditions are set to $R_{std} = 1000W/m^2$ and $T_{std} = 25^{\circ}C$. The temperature coefficient is set to $\alpha_p = -0.0035/^{\circ}C$. For **Wind Power**, we utilize the power curve of the widely deployed GE 2.5MW wind turbine. The wind speed at hub height (v_{hub}) is first extrapolated from the 10m wind speed ($v_{10m} \in c_t$) using the power law with a shear exponent $\alpha = 0.143$: $v_{hub} = v_{10m} \cdot (h_{hub}/10)^{\alpha}$, where $h_{hub} = 100m$. The power output is then interpolated from the manufacturer’s power curve (Figure 4).

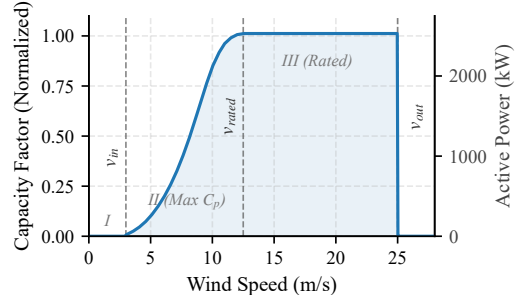


Figure 4: Power curve of the GE 2.5MW wind turbine. The curve illustrates the non-linear relationship between wind speed and power generation, highlighting three operational regions: cut-in ($v_{in} \approx 3$ m/s), rated ($v_{rated} \approx 12.5$ m/s), and cut-out ($v_{out} = 25$ m/s).

Autoregressive (AR) Models. These models generate predictions iteratively ($\hat{y}_{t+1} = f(y_t, h_t, c_{t+1})$) and are suitable for capturing sequential dependencies. We evaluate **RNN Variants** including standard **RNN** [9], **LSTM** [11], and **GRU** [7], along with their bidirectional counterparts [7, 11, 24] (**Bi-LSTM**, **Bi-GRU**). Future NWP data is injected at each decoding step.

Non-Autoregressive (NAR) Models. These models predict the entire horizon simultaneously and are widely considered State-of-the-Art (SOTA) in long-term time series forecasting. We evaluate three sub-categories: (i) **CNN-based:** **TCN** [3] and **TimesNet** [36], leveraging 1D or 2D convolutions to capture temporal variations; (ii) **MLP-based:** **DLinear** [43], **STID** [25], and **TSMixer** [6], which prioritize efficiency; and (iii) **Transformer-based:** **Autoformer** [37], **Informer** [47], and **iTransformer** [16], employing attention mechanisms to model global weather contexts.

4.3 Evaluation Metrics

To provide a comprehensive assessment, we employ standard statistical metrics, including Mean Absolute Error (MAE) and Root Mean Square Error (RMSE). However, purely statistical errors often fail to reflect the operational viability of forecasts in real-world power grids. Therefore, we adopt the Qualification Rate (Q), a standard industrial metric used to evaluate whether prediction errors remain within the safety tolerance thresholds required for grid dispatch and stability. Furthermore, absolute error metrics are inherently sensitive to the magnitude of the target variable. This magnitude dependence makes it difficult to fairly compare model robustness across different meteorological regimes. To address this limitation and explicitly quantify the value of our model against Physics-based baselines, we propose the Forecast Skill Score (S).

Industrial Qualification Rate (Q). Following power system standards, we utilize the Qualification Rate to measure the proportion of predictions that satisfy operational safety margins. Let τ denote the tolerance threshold (set to $\tau = 0.25$ in our experiments). The rate Q is defined as:

$$Q = \frac{1}{|\Omega_{\text{test}}|} \sum_{(t,i) \in \Omega_{\text{test}}} \mathbb{I}(|y_t^{(i)} - \hat{y}_t^{(i)}| \leq (1 - \tau)) \times 100\%, \quad (8)$$

where $\mathbb{I}(\cdot)$ is the indicator function, and Ω_{test} represents the set of all valid test samples. A higher Q indicates better compliance with grid dispatch requirements.

Forecast Skill Score (S). To explicitly quantify the value of our model against established baselines across different scenarios, we propose the Forecast Skill Score. This metric measures the percentage improvement of the deep learning models over a benchmark baseline (e.g., Physics-based or Persistence methods), defined as:

$$S = \left(1 - \frac{\text{MAE}_{\text{model}}}{\text{MAE}_{\text{baseline}}}\right) \times 100\%. \quad (9)$$

A positive S indicates the model outperforms the baseline, while a negative value implies degradation. Comparing S_{norm} and S_{ext} reveals whether the model maintains its predictive advantage under stress. Importantly, we select the *best-performing physics-based baseline* to ensure a conservative and industry-relevant evaluation. Specifically, we use physical conversion models for solar power forecasting and the standard GE 2.5MW turbine power curve for wind power forecasting.

4.4 Experimental Settings

All experiments are implemented in PyTorch and conducted on NVIDIA GPUs. To ensure reproducibility and prevent information leakage, each dataset is strictly split by time into Training, Validation, and Test sets with a ratio of 7:1:2. The target variable, power generation capacity factor, is naturally bounded within $[0, 1]$, while all meteorological covariates are standardized using Z-score normalization computed exclusively on the training set. Models are trained for a maximum of 20 epochs using the AdamW optimizer with a weight decay of 1×10^{-5} , and early stopping is applied with a patience of three epochs based on validation loss. We consider commonly used ranges for key hyperparameters, including learning rate $\in \{10^{-1}, \dots, 10^{-5}\}$ and dropout $\in \{0, 0.05, 0.1\}$ for all models; autoregressive models (RNN/LSTM/GRU) additionally vary

the number of layers in $[1, 2]$ and hidden size in $[128, 256]$; CNN and MLP models vary the number of layers in $[2, 4]$ and model dimension $d_{\text{model}} \in [32, 64, 128]$; and Transformer-based models vary encoder/decoder layers in $[1, 2]$ with $d_{\text{model}} \in [32, 64]$. For each model, we select the best-performing configuration. Each experiment is repeated five times with different random seeds, and we report the mean and standard deviation of all evaluation metrics.

5 Experimental Results and Analysis

5.1 Overall Performance

In this section, we present a comprehensive analysis of the forecasting performance across 16 models on the R²Energy datasets, focusing on the overall hierarchy, temporal sensitivity, modality characteristics, and operational reliability. The results are shown in Table 4 and Table 5.

Overall Performance Hierarchy. A macro-level inspection of in Table 4 and Table 5 reveals a clear hierarchy: deep learning models substantially outperform statistical and physics-based baselines. For example, in the Solar S1 dataset (Panel A), the best-performing deep learning models achieve an MAE of approximately 0.052, representing a reduction of over 50% compared to the physical baseline (MAE 0.1283). However, beyond this expected gap, R²Energy exposes a fundamental trend: performance is governed less by model complexity and more by the alignment between the architecture and the data-generating process. Across both wind and solar datasets, Autoregressive (AR) models, particularly GRU and Bi-GRU, emerge as consistent leaders. In the ultra-short-term forecast (Horizon=1), GRU achieves the lowest MAE on the W1 (0.0567), S1 (0.0527), and S2 (0.0541) datasets. This advantage stems from their decoding paradigm. In R²Energy, renewable generation is treated as an NWP-assisted mapping task where meteorological covariates are available at every step. AR models inject these signals dynamically during decoding, preserving a tight temporal coupling between instantaneous weather forcing and power output. In contrast, Transformer-based models, which rely on global attention, often struggle to filter high-frequency stochastic fluctuations in low signal-to-noise regimes. Consequently, models like Autoformer significantly underperform simpler RNN variants in wind datasets (e.g., W1 MAE 0.2078 vs. GRU 0.0567).

Impact of Forecasting Horizons. The relative strengths of model families evolve systematically with forecasting horizon, revealing how NWP availability reshapes classical horizon-dependent trade-offs. (i) **Ultra-Short-Term (USTF, 1h):** In the immediate reaction regime, AR models dominate across nearly all datasets (e.g., GRU ranking first in W1, S1–S3). At this horizon, the most recent system state y_t remains highly informative, and recursive decoding benefits from strong short-term autocorrelation. The superiority of AR models here reflects their ability to directly exploit local temporal continuity; (ii) **Short-Term (STF, 24h):** Contrary to the conventional expectation that AR models suffer from cumulative error, GRU-based models maintain their leading positions in the day-ahead setting. This observation is critical: future NWP signals act as an external correction mechanism, effectively anchoring the recursive trajectory to physically plausible weather evolutions. As a result, error propagation is substantially mitigated, and AR models

Table 4: Prediction results on three Datasets (S1, S2, S3). The Baseline corresponds to a physics-informed photovoltaic formulation and the Seasonal-Naive method, respectively. The tasks are categorized into three Panels based on forecast horizons. Results are formatted as Mean (Std). Darker background indicates better performance (Rank 1 to 4).

Model	S1			S2			S3		
	MAE ↓	RMSE ↓	Q (%) ↑	MAE ↓	RMSE ↓	Q (%) ↑	MAE ↓	RMSE ↓	Q (%) ↑
<i>Panel A: Ultra-short-term Forecast (Horizon = 1)</i>									
Baseline	0.1283/0.1318	0.1725/0.2151	86.41/80.89	0.1760/0.1545	0.2346/0.2490	72.33/76.39	0.1166/0.1274	0.1717/0.2054	86.75/82.40
RNN	0.0527 (0.001)	0.0866 (0.000)	97.70 (0.026)	0.0576 (0.003)	0.0964 (0.003)	96.78 (0.217)	0.0570 (0.001)	0.0888 (0.001)	97.57 (0.047)
LSTM	0.2170 (0.135)	0.2997 (0.174)	69.83 (22.70)	0.2034 (0.124)	0.2930 (0.164)	71.52 (20.78)	0.1744 (0.098)	0.2536 (0.137)	76.18 (17.56)
Bi-LSTM	0.1628 (0.134)	0.2289 (0.174)	79.12 (22.72)	0.1541 (0.123)	0.2268 (0.164)	80.01 (20.78)	0.1348 (0.098)	0.1981 (0.136)	83.35 (17.56)
GRU	0.0527 (0.001)	0.0864 (0.000)	97.72 (0.010)	0.0541 (0.002)	0.0930 (0.002)	96.96 (0.091)	0.0564 (0.001)	0.0880 (0.001)	97.61 (0.049)
Bi-GRU	0.0528 (0.001)	0.0866 (0.000)	97.71 (0.017)	0.0533 (0.000)	0.0917 (0.001)	97.08 (0.037)	0.0554 (0.001)	0.0871 (0.000)	97.67 (0.022)
TCN	0.2270 (0.000)	0.3416 (0.000)	61.30 (0.000)	0.2052 (0.121)	0.2941 (0.163)	71.50 (20.75)	0.1753 (0.097)	0.2544 (0.136)	76.18 (17.56)
TimesNet	0.0610 (0.002)	0.0949 (0.002)	97.30 (0.107)	0.0644 (0.002)	0.1046 (0.002)	96.22 (0.210)	0.0599 (0.001)	0.0916 (0.001)	97.44 (0.069)
DLinear	0.1670 (0.101)	0.2212 (0.126)	76.31 (21.23)	0.1602 (0.057)	0.2074 (0.061)	78.31 (12.58)	0.1747 (0.044)	0.2370 (0.054)	74.32 (10.58)
STID	0.1096 (0.109)	0.1603 (0.141)	88.20 (18.45)	0.0685 (0.005)	0.1075 (0.006)	96.00 (0.516)	0.0963 (0.079)	0.1445 (0.110)	90.35 (14.26)
TSMixer	0.0595 (0.002)	0.0927 (0.002)	97.42 (0.171)	0.0650 (0.001)	0.1042 (0.002)	96.30 (0.319)	0.0607 (0.002)	0.0920 (0.002)	97.45 (0.164)
Autoformer	0.1335 (0.006)	0.1837 (0.007)	81.78 (1.579)	0.1706 (0.109)	0.2428 (0.151)	78.67 (19.70)	0.1565 (0.080)	0.2260 (0.114)	80.17 (14.97)
Informer	0.0838 (0.003)	0.1236 (0.002)	94.01 (0.178)	0.1311 (0.087)	0.1921 (0.118)	85.07 (15.26)	0.0736 (0.002)	0.1090 (0.003)	95.86 (0.308)
iTransformer	0.0580 (0.001)	0.0926 (0.001)	97.29 (0.080)	0.0666 (0.001)	0.1070 (0.002)	95.53 (0.178)	0.0616 (0.000)	0.0931 (0.001)	97.26 (0.068)
<i>Panel B: Short-term Forecast (Horizon = 24)</i>									
Baseline	0.1272/0.1303	0.1702/0.2127	86.79/81.12	0.1731/0.1530	0.2305/0.2464	72.91/76.61	0.1143/0.1247	0.1683/0.2010	87.25/82.86
RNN	0.0859 (0.001)	0.1303 (0.000)	93.63 (0.036)	0.1032 (0.001)	0.1560 (0.001)	89.01 (0.253)	0.0928 (0.001)	0.1373 (0.001)	91.78 (0.239)
LSTM	0.1359 (0.096)	0.1942 (0.124)	84.82 (16.89)	0.1035 (0.002)	0.1577 (0.001)	89.04 (0.316)	0.1227 (0.064)	0.1801 (0.090)	86.13 (11.90)
Bi-LSTM	0.1844 (0.118)	0.2565 (0.152)	76.35 (20.66)	0.1842 (0.099)	0.2654 (0.132)	75.10 (16.85)	0.1542 (0.079)	0.2251 (0.111)	80.15 (14.55)
GRU	0.0844 (0.001)	0.1297 (0.001)	93.69 (0.032)	0.1022 (0.001)	0.1550 (0.000)	89.41 (0.124)	0.0889 (0.001)	0.1333 (0.000)	92.36 (0.039)
Bi-GRU	0.0858 (0.001)	0.1319 (0.001)	93.32 (0.198)	0.1035 (0.002)	0.1560 (0.001)	89.30 (0.236)	0.0893 (0.001)	0.1339 (0.001)	92.23 (0.086)
TCN	0.0910 (0.001)	0.1354 (0.001)	92.84 (0.083)	0.1146 (0.002)	0.1675 (0.001)	86.75 (0.310)	0.0987 (0.001)	0.1430 (0.001)	91.13 (0.176)
TimesNet	0.0904 (0.001)	0.1359 (0.001)	92.67 (0.169)	0.1180 (0.005)	0.1733 (0.008)	85.87 (0.788)	0.0975 (0.000)	0.1417 (0.001)	91.28 (0.098)
DLinear	0.0885 (0.003)	0.1306 (0.003)	93.40 (0.477)	0.1259 (0.011)	0.1767 (0.012)	84.10 (2.731)	0.0943 (0.003)	0.1388 (0.004)	91.69 (0.507)
STID	0.1878 (0.115)	0.2607 (0.149)	75.60 (20.11)	0.1730 (0.069)	0.2454 (0.096)	75.84 (11.53)	0.1290 (0.061)	0.1859 (0.087)	85.55 (11.62)
TSMixer	0.0982 (0.007)	0.1438 (0.009)	91.18 (1.631)	0.1321 (0.011)	0.1904 (0.017)	82.37 (2.613)	0.1023 (0.004)	0.1485 (0.006)	90.11 (1.013)
Autoformer	0.1228 (0.007)	0.1729 (0.007)	85.34 (1.792)	0.1657 (0.070)	0.2316 (0.098)	76.67 (11.17)	0.1045 (0.003)	0.1518 (0.001)	90.09 (0.093)
Informer	0.0929 (0.001)	0.1361 (0.001)	92.11 (0.125)	0.1734 (0.066)	0.2379 (0.095)	76.20 (10.91)	0.1023 (0.002)	0.1500 (0.002)	90.08 (0.272)
iTransformer	0.0982 (0.001)	0.1425 (0.001)	90.87 (0.157)	0.1238 (0.002)	0.1746 (0.001)	84.66 (0.291)	0.0946 (0.000)	0.1389 (0.000)	91.55 (0.031)
<i>Panel C: Medium-term Forecast (Horizon = 72)</i>									
Baseline	0.1273/0.3262	0.1694/0.4254	86.91/49.05	0.1698/0.3126	0.2260/0.4208	73.63/51.82	0.1128/0.2489	0.1661/0.3467	87.53/61.86
RNN	0.0861 (0.003)	0.1311 (0.002)	93.59 (0.326)	0.1077 (0.005)	0.1612 (0.004)	88.05 (1.061)	0.0918 (0.001)	0.1358 (0.002)	91.70 (0.356)
LSTM	0.0875 (0.001)	0.1332 (0.001)	93.33 (0.154)	0.1047 (0.001)	0.1610 (0.002)	88.68 (0.283)	0.1217 (0.062)	0.1786 (0.088)	86.14 (11.38)
Bi-LSTM	0.1880 (0.123)	0.2609 (0.155)	75.52 (21.32)	0.1880 (0.123)	0.2609 (0.155)	75.52 (21.32)	0.1524 (0.076)	0.2231 (0.107)	80.29 (13.81)
GRU	0.0858 (0.003)	0.1309 (0.002)	93.69 (0.278)	0.1003 (0.001)	0.1563 (0.002)	89.62 (0.317)	0.0906 (0.002)	0.1337 (0.001)	92.04 (0.135)
Bi-GRU	0.0893 (0.001)	0.1383 (0.001)	92.23 (0.198)	0.0990 (0.001)	0.1545 (0.000)	89.88 (0.145)	0.0898 (0.001)	0.1342 (0.001)	91.88 (0.283)
TCN	0.0917 (0.001)	0.1362 (0.001)	92.69 (0.161)	0.1230 (0.001)	0.1773 (0.001)	84.86 (0.335)	0.1022 (0.001)	0.1444 (0.000)	90.75 (0.083)
TimesNet	0.0920 (0.001)	0.1367 (0.001)	92.69 (0.185)	0.1216 (0.001)	0.1772 (0.001)	85.10 (0.111)	0.0996 (0.001)	0.1450 (0.001)	90.45 (0.223)
DLinear	0.0874 (0.003)	0.1291 (0.003)	93.84 (0.450)	0.1270 (0.007)	0.1756 (0.008)	84.16 (2.190)	0.0990 (0.003)	0.1414 (0.005)	91.16 (0.672)
STID	0.2897 (0.097)	0.3893 (0.123)	57.90 (17.02)	0.1759 (0.065)	0.2485 (0.090)	74.35 (10.03)	0.1605 (0.069)	0.2296 (0.102)	79.60 (13.26)
TSMixer	0.0975 (0.010)	0.1436 (0.012)	91.25 (2.436)	0.1338 (0.010)	0.1919 (0.015)	81.57 (2.387)	0.1124 (0.012)	0.1600 (0.016)	87.67 (3.457)
Autoformer	0.1126 (0.003)	0.1580 (0.003)	87.83 (0.673)	0.1689 (0.069)	0.2328 (0.098)	75.31 (10.53)	0.1003 (0.002)	0.1478 (0.001)	90.13 (0.124)
Informer	0.0838 (0.003)	0.1236 (0.002)	94.01 (0.178)	0.1501 (0.078)	0.2170 (0.106)	81.32 (13.50)	0.0957 (0.001)	0.1397 (0.001)	91.08 (0.267)
iTransformer	0.0987 (0.001)	0.1420 (0.001)	91.13 (0.214)	0.1295 (0.002)	0.1799 (0.002)	82.61 (0.486)	0.0958 (0.001)	0.1405 (0.001)	91.00 (0.163)

retain stability even over 24 steps; (iii) **Medium-Term (MTF, 72h)**: At longer horizons, performance gaps narrow. While AR models remain competitive, Non-Autoregressive (NAR) architectures such as TimesNet and TCN become increasingly viable, particularly in volatile wind datasets (e.g., surpassing LSTM in W3). This transition suggests that when immediate historical states lose predictive power, models that emphasize global temporal patterns and multi-periodicity gain relative advantage. R²Energy thus highlights a

regime-dependent crossover rather than a single universally optimal architecture.

The relative strengths of model families evolve systematically with the forecasting horizon. (i) **Ultra-Short-Term (1h)**: In the immediate reaction regime, AR models dominate. For instance, in Table 4, GRU and RNN variants consistently rank first across S1–S3. At this horizon, the most recent system state y_t is highly informative, and recursive decoding exploits local temporal continuity effectively. (ii) **Short-Term (24h)**: Contrary to the expectation that

Table 5: Prediction results on three Datasets (W1, W2, W3). The Baseline corresponds to a turbine power-curve-based formulation and the Seasonal-Naive method, respectively. The tasks are categorized into three Panels based on forecast horizons. Results are formatted as Mean (Std). Darker background indicates better performance (Rank 1 to 4).

Model	W1			W2			W3		
	MAE ↓	RMSE ↓	Q (%) ↑	MAE ↓	RMSE ↓	Q (%) ↑	MAE ↓	RMSE ↓	Q (%) ↑
<i>Panel A: Ultra-short-term Forecast (Horizon = 1)</i>									
Baseline	0.2042/0.2106	0.2975/0.2934	66.86/-	0.2544/0.2546	0.3650/0.3451	61.07/59.58	0.1443/0.1747	0.2220/0.2480	80.01/74.68
RNN	0.0586 (0.001)	0.0889 (0.000)	97.85 (0.050)	0.0627 (0.001)	0.0957 (0.000)	97.29 (0.032)	0.0600 (0.001)	0.0939 (0.001)	97.31 (0.055)
LSTM	0.1761 (0.098)	0.2536 (0.137)	74.64 (13.70)	0.2019 (0.114)	0.2889 (0.159)	72.88 (20.00)	0.1398 (0.053)	0.2048 (0.080)	81.98 (11.93)
Bi-LSTM	0.1364 (0.097)	0.1979 (0.137)	80.21 (13.68)	0.1555 (0.114)	0.2241 (0.159)	81.06 (20.01)	0.1168 (0.054)	0.1693 (0.082)	87.15 (12.17)
GRU	0.0567 (0.001)	0.0863 (0.001)	98.05 (0.060)	0.0618 (0.001)	0.0942 (0.001)	97.40 (0.069)	0.0657 (0.001)	0.0984 (0.001)	97.10 (0.043)
Bi-GRU	0.0567 (0.000)	0.0867 (0.001)	98.02 (0.081)	0.0614 (0.001)	0.0936 (0.001)	97.45 (0.054)	0.0662 (0.001)	0.0969 (0.001)	97.32 (0.053)
TCN	0.0591 (0.000)	0.0893 (0.000)	97.92 (0.030)	0.0638 (0.000)	0.0972 (0.000)	97.23 (0.034)	0.1407 (0.023)	0.1829 (0.023)	82.53 (5.961)
TimesNet	0.0578 (0.001)	0.0884 (0.002)	97.89 (0.114)	0.0623 (0.000)	0.0944 (0.000)	97.43 (0.036)	0.0922 (0.008)	0.1336 (0.005)	93.38 (0.791)
DLinear	0.1360 (0.026)	0.1822 (0.030)	85.27 (4.517)	0.0892 (0.051)	0.1253 (0.058)	92.35 (7.973)	0.2018 (0.017)	0.2673 (0.013)	66.31 (7.949)
STID	0.1296 (0.066)	0.1863 (0.093)	84.45 (13.12)	0.0645 (0.002)	0.0990 (0.003)	97.04 (0.185)	0.1519 (0.020)	0.2181 (0.029)	78.84 (4.221)
TSMixer	0.0662 (0.004)	0.1006 (0.007)	96.97 (0.640)	0.0650 (0.001)	0.0986 (0.001)	97.15 (0.091)	0.1066 (0.017)	0.1599 (0.022)	88.97 (3.717)
Autoformer	0.2078 (0.043)	0.2993 (0.060)	67.50 (7.457)	0.1525 (0.001)	0.2117 (0.001)	78.47 (0.224)	0.3092 (0.254)	0.3837 (0.229)	58.33 (28.06)
Informer	0.0942 (0.001)	0.1363 (0.001)	92.17 (0.262)	0.0941 (0.001)	0.1370 (0.001)	92.30 (0.187)	0.1428 (0.035)	0.1898 (0.039)	82.52 (8.518)
iTransformer	0.0888 (0.009)	0.1315 (0.014)	92.81 (1.842)	0.1090 (0.014)	0.1529 (0.019)	90.00 (2.692)	0.1455 (0.019)	0.1837 (0.019)	82.55 (5.026)
<i>Panel B: Short-term Forecast (Horizon = 24)</i>									
Baseline	0.2023/0.2084	0.2950/0.2907	67.23/67.38	0.2540/0.2538	0.3649/0.3441	61.20/59.73	0.1424/0.1721	0.2184/0.2449	80.36/75.15
RNN	0.1067 (0.001)	0.1505 (0.001)	89.89 (0.135)	0.1501 (0.002)	0.2010 (0.002)	81.37 (0.434)	0.1221 (0.002)	0.1702 (0.001)	86.66 (0.245)
LSTM	0.1363 (0.059)	0.1937 (0.084)	83.78 (11.81)	0.1491 (0.001)	0.1988 (0.000)	81.66 (0.287)	0.1516 (0.015)	0.2018 (0.032)	81.00 (4.260)
Bi-LSTM	0.1657 (0.072)	0.2359 (0.103)	77.90 (14.48)	0.2073 (0.072)	0.2869 (0.108)	71.60 (12.18)	0.1588 (0.017)	0.2181 (0.039)	78.77 (5.022)
GRU	0.1062 (0.000)	0.1507 (0.000)	89.81 (0.110)	0.1458 (0.002)	0.1958 (0.001)	82.10 (0.333)	0.1251 (0.001)	0.1699 (0.001)	86.43 (0.150)
Bi-GRU	0.1080 (0.000)	0.1529 (0.001)	89.48 (0.164)	0.1497 (0.001)	0.1998 (0.001)	81.27 (0.262)	0.1300 (0.003)	0.1744 (0.002)	85.33 (0.521)
TCN	0.1131 (0.000)	0.1608 (0.000)	88.12 (0.084)	0.1580 (0.001)	0.2092 (0.001)	79.56 (0.142)	0.1420 (0.006)	0.1857 (0.005)	82.69 (1.835)
TimesNet	0.1115 (0.001)	0.1587 (0.001)	88.52 (0.135)	0.1549 (0.001)	0.2072 (0.001)	80.05 (0.270)	0.1475 (0.007)	0.1940 (0.006)	80.72 (1.521)
DLinear	0.1178 (0.003)	0.1630 (0.005)	88.12 (0.639)	0.1633 (0.012)	0.2124 (0.012)	78.28 (2.855)	0.1779 (0.044)	0.2298 (0.057)	75.36 (9.449)
STID	0.1768 (0.054)	0.2497 (0.080)	74.69 (10.86)	0.1720 (0.011)	0.2294 (0.020)	76.10 (2.855)	0.1879 (0.028)	0.2569 (0.041)	71.31 (6.736)
TSMixer	0.1307 (0.013)	0.1902 (0.021)	83.53 (3.163)	0.1593 (0.001)	0.2128 (0.003)	79.01 (0.307)	0.1659 (0.017)	0.2437 (0.026)	76.17 (3.102)
Autoformer	0.2119 (0.051)	0.3051 (0.070)	67.47 (8.944)	0.1891 (0.001)	0.2634 (0.001)	70.77 (0.137)	0.1802 (0.000)	0.2665 (0.000)	72.63 (0.016)
Informer	0.1292 (0.001)	0.1805 (0.002)	84.39 (0.295)	0.1638 (0.001)	0.2160 (0.001)	78.18 (0.175)	0.1412 (0.009)	0.1902 (0.007)	83.54 (1.689)
iTransformer	0.1212 (0.002)	0.1755 (0.002)	85.92 (0.351)	0.1696 (0.005)	0.2198 (0.005)	76.64 (1.047)	0.1487 (0.026)	0.1955 (0.023)	80.39 (6.299)
<i>Panel C: Medium-term Forecast (Horizon = 72)</i>									
Baseline	0.2004/0.2626	0.2927/0.3475	67.61/57.43	0.2499/0.2863	0.3612/0.3805	61.95/54.97	0.1424/0.1955	0.2180/0.2690	80.34/70.29
RNN	0.1116 (0.002)	0.1575 (0.002)	88.81 (0.390)	0.1628 (0.003)	0.2140 (0.003)	78.62 (0.694)	0.1275 (0.005)	0.1737 (0.003)	85.83 (0.809)
LSTM	0.1384 (0.054)	0.1959 (0.080)	80.41 (7.989)	0.1582 (0.002)	0.2097 (0.001)	79.59 (0.344)	0.1411 (0.006)	0.1833 (0.005)	83.67 (1.323)
Bi-LSTM	0.1651 (0.067)	0.2355 (0.098)	76.45 (9.814)	0.2101 (0.066)	0.2910 (0.102)	71.17 (10.92)	0.1642 (0.017)	0.2255 (0.036)	77.02 (4.667)
GRU	0.1088 (0.000)	0.1536 (0.001)	89.36 (0.154)	0.1524 (0.002)	0.2047 (0.001)	80.62 (0.294)	0.1322 (0.005)	0.1760 (0.004)	84.93 (1.052)
Bi-GRU	0.1098 (0.001)	0.1551 (0.001)	89.08 (0.129)	0.1536 (0.003)	0.2050 (0.003)	80.38 (0.481)	0.1447 (0.009)	0.1892 (0.010)	81.63 (2.589)
TCN	0.1171 (0.001)	0.1674 (0.001)	87.19 (0.203)	0.1720 (0.003)	0.2267 (0.002)	76.39 (0.653)	0.1425 (0.014)	0.1893 (0.012)	81.83 (3.450)
TimesNet	0.1176 (0.002)	0.1673 (0.002)	87.00 (0.315)	0.1723 (0.003)	0.2284 (0.002)	76.12 (0.704)	0.1331 (0.005)	0.1825 (0.005)	84.05 (1.227)
DLinear	0.1222 (0.007)	0.1676 (0.008)	87.71 (0.957)	0.1735 (0.012)	0.2226 (0.011)	76.83 (2.228)	0.2054 (0.032)	0.2503 (0.045)	67.11 (7.259)
STID	0.1224 (0.005)	0.1723 (0.003)	86.58 (0.537)	0.1786 (0.001)	0.2315 (0.000)	75.66 (0.105)	0.1987 (0.051)	0.2847 (0.063)	70.34 (8.213)
TSMixer	0.1575 (0.046)	0.2234 (0.066)	79.07 (8.922)	0.1732 (0.011)	0.2337 (0.020)	75.73 (2.483)	0.1830 (0.029)	0.2606 (0.039)	72.56 (5.708)
Autoformer	0.1869 (0.049)	0.2694 (0.071)	72.04 (8.699)	0.2078 (0.041)	0.2895 (0.063)	69.07 (5.636)	0.1756 (0.015)	0.2578 (0.021)	73.61 (3.130)
Informer	0.1219 (0.001)	0.1747 (0.002)	85.71 (0.376)	0.1634 (0.001)	0.2190 (0.001)	78.25 (0.254)	0.1415 (0.006)	0.1875 (0.006)	83.73 (1.115)
iTransformer	0.1187 (0.001)	0.1722 (0.002)	86.70 (0.298)	0.1731 (0.003)	0.2238 (0.002)	75.73 (0.552)	0.1448 (0.021)	0.1920 (0.019)	81.42 (4.999)

AR models suffer from error accumulation, GRU-based models maintain their lead. In Table 5 (Panel B), GRU achieves an MAE of 0.1062 on W1, significantly outperforming the best Transformer model (iTransformer, MAE 0.1212). This stability suggests that future NWP signals act as an external correction mechanism, anchoring the recursive trajectory to physically plausible weather evolutions. (iii) **Medium-Term (72h):** At longer horizons, performance gaps narrow. While AR models remain competitive, Non-Autoregressive (NAR) architectures like TimesNet begin to show advantages in

volatile datasets (e.g., W3), where they capture multi-scale temporal patterns that recursive methods may miss.

Modality-Specific Characteristics. R²Energy validates that "Wind" and "Solar" constitute distinct physical modalities requiring different modeling capabilities. Solar Power (S1–S3) operates in a pattern-dominant regime. Governed by deterministic diurnal cycles and direct irradiance relationships, solar datasets exhibit high predictability, reflected in consistently high qualification rates (Q >

90% for top models). In this setting, most competent deep learning models converge to similar performance ceilings, and architectural sophistication yields diminishing returns. Temporal consistency and accurate phase alignment, rather than expressive capacity, become the dominant factors. Wind Power (W1–W3), by contrast, represents a noise-dominant regime. As characterized in Section 3.1, datasets such as W2 and W3 exhibit strong diurnal asymmetry and high variance driven by turbulence and synoptic transitions. Here, overall Q-scores drop to 60–80%, and model rankings compress significantly. The relative improvement of CNN-based models (e.g., TCN) in wind tasks suggests that local receptive fields are effective for capturing short-lived gust structures and regime shifts, a property less critical in solar forecasting. This modality gap underscores why benchmarking across both wind and solar is essential for assessing generalizable forecasting robustness.

Training Stability and Industrial Reliability. Beyond average accuracy, R²Energy emphasizes training stability as a first-class evaluation dimension for safety-critical deployment. The reported standard deviations across five independent runs reveal stark contrasts between model families. Lightweight architectures, particularly GRU, Bi-GRU, and MLP-based models, exhibit highly stable convergence surfaces, with Std values typically below 0.002 in solar datasets. Such determinism is crucial for operational environments where retraining and redeployment are routine. In contrast, Transformer-based models demonstrate pronounced volatility, especially in high-noise wind regimes (e.g., Autoformer exhibiting $\text{Std} = 0.254$ in W3 USTF). This instability indicates a rugged optimization landscape exacerbated by stochastic meteorological inputs and limited effective signal. From an industrial perspective, such variance poses tangible risks: inconsistent model behavior under retraining undermines trust and complicates system integration. Collectively, these results suggest that robustness in renewable energy forecasting is not synonymous with architectural complexity, and that stability-aware benchmarks like R²Energy are necessary to bridge the gap between academic performance and operational reliability.

5.2 Robustness Under Extreme Weather

In this section, we conduct a fine-grained diagnostic analysis of model robustness under extreme meteorological regimes. We focus on the Short-Term Forecasting task ($H = 24$) for Solar (S1) and Wind (W1) datasets (shown in Table 6). To differentiate between "high-impact" and "high-difficulty" scenarios, we categorize events by their entropic nature and report three metrics: **MAE** (physical error), **Qualification Rate** (Q) (compliance with industrial safety margins), and **Forecast Skill Score** (S) (improvement relative to the physics-based baseline).

Solar Power (S1): The Low-Entropy Extreme. The results on S1 reveal a "Clear-Sky Paradox." During **Heatwave** events, we observe a universal performance improvement compared to the Normal regime. For instance, the leading GRU model reduces its MAE from 0.0871 (Normal) to 0.0680 (Heatwave), with the Qualification Rate (Q) approaching near-perfect levels (97.51%). This improvement highlights that heatwaves, while operationally critical, represent a *low-entropy* forecasting task: they are typically

accompanied by stable, cloud-free conditions. In this deterministic regime, Deep Learning models successfully capture the non-linear temperature-derating coefficients, significantly outperforming the physical Baseline (Skill Score $S = 45.68\%$). Conversely, **Rainstorm** events introduce a *high-entropy* regime dominated by dynamic cloud occlusion. While absolute MAE values decrease due to suppressed total output, the relative Skill Scores expose architectural fragilities. The Baseline fails to track rapid cloud transients. Under these conditions, Autoregressive (AR) models (RNN/GRU) maintain robustness ($S \approx 10 - 31\%$, $Q > 97\%$). In stark contrast, Transformer-based architectures exhibit instability; the Autoformer degrades to a negative Skill Score ($S = -26.06\%$), performing worse than the primitive physical baseline. This suggests that global attention mechanisms, while effective for semantic context, struggle to model the local, high-frequency "shading" effects inherent to rainstorms.

Wind Power (W1): Turbulence and the Robustness Gap. The Wind (W1) dataset presents a rigorous stress test characterized by non-stationary regime shifts. The distinction between model classes becomes stark under Rainstorm conditions (Panel B), where the physical Baseline suffers a catastrophic collapse (MAE: 0.2720, $Q: 27\text{--}49\%$). This underscores the inability of static power curves to account for convective turbulence. In this high-noise regime, we identify a decisive "Robustness Gap." The GRU and Bi-GRU models demonstrate exceptional resilience (MAE ≈ 0.15 , $Q \approx 80\%$), achieving a massive Skill Score improvement of over 40%. Notably, the TCN also performs strongly ($S = 44.96\%$), suggesting that architectures with local receptive fields are well-suited for capturing short-lived gust features. However, the Autoformer collapses ($S = -78.57\%$, $Q = 31.26\%$). This indicates that during high-entropy wind events, global correlation modeling tends to interpret high-frequency turbulence as noise to be smoothed, leading to under-dispersed and operationally dangerous predictions.

Diagnostic Summary: Alignment of Inductive Bias. The cross-comparison leads to a critical finding: architectural complexity does not correlate with operational robustness in NWP-driven tasks. Simple, lightweight recurrent architectures (GRU/RNN) consistently outperform complex Transformers in high-stakes weather scenarios. We attribute this to the alignment between the model's inductive bias and the physical task: power generation during a storm is a causal, step-wise reaction to immediate meteorological forcing. AR models, which inject NWP data dynamically at each decoding step, mirror this physical causality. Conversely, generative Non-Autoregressive models appear prone to *signal dilution*, where the precise NWP forcing at time t is washed out by the global attention mechanism, rendering them less reliable for safety-critical dispatch.

5.3 Operational Efficiency

Beyond predictive accuracy, the deployment of forecasting models in real-time grid dispatch systems is constrained by strict latency budgets and computational resource limits. Figure 5 presents a cost-benefit analysis on the Solar (S1) dataset ($H = 24$), plotting MAE against per-epoch training cost (seconds, log scale). The results challenge the prevailing trend toward increasingly deep architectures. The bottom-left quadrant of the efficiency landscape,

Table 6: Robustness Evaluation under Extreme Weather Conditions (Task: Short-Term Forecasting, H=24). We report the MAE, Qualification Rate (Q), and Forecast Skill Score (S). S measures the relative improvement over the Baseline; higher S indicates better performance. The Baseline corresponds to a physics-informed photovoltaic formulation and the Seasonal-Naive method. Results are formatted as Mean (Std). Darker background indicates better performance (Rank 1 to 4).

Model	Normal			Heatwave			Rainstorm		
	MAE ↓	Q (%) ↑	S (%) ↑	MAE ↓	Q (%) ↑	S (%) ↑	MAE ↓	Q (%) ↑	S (%) ↑
<i>Panel A: Short-term Forecast (Horizon = 24) on S1</i>									
Baseline	0.1269/0.1397	86.10/79.36	0.00 (–)	0.1309/0.0697	90.67/92.39	0.00 (–)	0.0687/0.2064	95.93/70.46	0.00 (–)
RNN	0.0885 (0.001)	92.97 (0.045)	30.26 (0.788)	0.0711 (0.001)	97.54 (0.105)	45.68 (0.764)	0.0615 (0.002)	97.29 (0.310)	10.48 (2.911)
LSTM	0.1350 (0.089)	84.66 (15.81)	-6.38 (70.13)	0.1437 (0.145)	85.36 (24.10)	-9.78 (110.7)	0.0730 (0.009)	96.13 (1.990)	-6.26 (13.10)
Bi-LSTM	0.1799 (0.108)	76.72 (19.33)	-41.77 (85.11)	0.2168 (0.177)	73.27 (29.49)	-65.62 (135.2)	0.0760 (0.012)	95.16 (2.454)	-10.63 (17.46)
GRU	0.0871 (0.001)	93.05 (0.039)	31.36 (0.788)	0.0680 (0.002)	97.51 (0.065)	48.05 (1.528)	0.0680 (0.004)	97.09 (0.363)	1.02 (5.822)
Bi-GRU	0.0887 (0.001)	92.64 (0.218)	30.10 (0.788)	0.0685 (0.002)	97.37 (0.068)	47.67 (1.528)	0.0691 (0.002)	97.03 (0.235)	-0.58 (2.911)
TCN	0.0940 (0.000)	92.12 (0.091)	25.93 (0.000)	0.0727 (0.002)	97.28 (0.048)	44.46 (1.528)	0.0816 (0.001)	93.69 (0.151)	-18.78 (1.456)
TimesNet	0.0936 (0.001)	91.94 (0.158)	26.24 (0.788)	0.0709 (0.004)	97.07 (0.374)	45.84 (3.056)	0.0809 (0.001)	93.60 (0.230)	-17.76 (1.456)
DLinear	0.0911 (0.003)	92.78 (0.492)	28.21 (2.364)	0.0730 (0.003)	97.08 (0.409)	44.23 (2.292)	0.0745 (0.006)	96.53 (0.509)	-8.44 (8.733)
STID	0.1840 (0.105)	75.95 (18.76)	-45.00 (82.74)	0.2149 (0.179)	72.82 (29.11)	-64.17 (136.7)	0.0904 (0.007)	92.48 (1.220)	-31.59 (10.19)
TSMixer	0.1018 (0.008)	90.24 (1.867)	19.78 (6.304)	0.0762 (0.005)	96.87 (0.286)	41.79 (3.820)	0.0850 (0.004)	93.07 (0.718)	-23.73 (5.822)
Autoformer	0.1272 (0.008)	83.88 (2.165)	-0.24 (6.304)	0.0968 (0.003)	94.10 (0.590)	26.05 (2.292)	0.0866 (0.001)	92.93 (0.205)	-26.06 (1.456)
Informer	0.0958 (0.001)	91.28 (0.150)	24.51 (0.788)	0.0762 (0.003)	97.11 (0.266)	41.79 (2.292)	0.0688 (0.002)	96.76 (0.285)	-0.15 (2.911)
iTransformer	0.1013 (0.001)	89.99 (0.173)	20.17 (0.788)	0.0795 (0.002)	96.23 (0.138)	39.27 (1.528)	0.0795 (0.002)	94.32 (0.363)	-15.72 (2.911)
<i>Panel B: Short-term Forecast (Horizon = 24) on W1</i>									
Baseline	0.2023/0.2129	67.23/66.47	0.00 (–)	0.1638/0.1573	74.37/77.65	0.00 (–)	0.2720/0.4203	49.68/27.67	0.00 (–)
RNN	0.1076 (0.001)	89.62 (0.162)	46.81 (0.494)	0.0962 (0.002)	92.74 (0.109)	41.27 (1.221)	0.1510 (0.008)	81.25 (2.743)	44.49 (2.941)
LSTM	0.1378 (0.060)	83.43 (12.06)	31.88 (29.66)	0.1154 (0.038)	88.06 (8.796)	29.55 (23.20)	0.2636 (0.194)	63.37 (26.18)	3.09 (71.32)
Bi-LSTM	0.1681 (0.073)	77.40 (14.77)	16.91 (36.08)	0.1338 (0.046)	83.93 (10.99)	18.32 (28.08)	0.3628 (0.235)	49.52 (31.43)	-33.38 (86.39)
GRU	0.1071 (0.000)	89.52 (0.116)	47.06 (0.000)	0.0953 (0.001)	92.94 (0.151)	41.82 (0.611)	0.1595 (0.008)	78.73 (1.605)	41.36 (2.941)
Bi-GRU	0.1091 (0.000)	89.16 (0.167)	46.07 (0.000)	0.0964 (0.001)	92.79 (0.465)	41.15 (0.611)	0.1529 (0.008)	79.69 (1.205)	43.79 (2.941)
TCN	0.1140 (0.000)	87.90 (0.121)	43.65 (0.000)	0.0966 (0.000)	91.73 (0.134)	41.03 (0.000)	0.1497 (0.006)	80.54 (1.427)	44.96 (2.206)
TimesNet	0.1130 (0.001)	88.18 (0.152)	44.14 (0.494)	0.0953 (0.001)	92.04 (0.039)	41.82 (0.611)	0.1533 (0.002)	79.81 (0.512)	43.64 (0.735)
DLinear	0.1195 (0.003)	87.73 (0.644)	40.93 (1.483)	0.1018 (0.003)	92.17 (0.679)	37.85 (1.832)	0.1566 (0.010)	78.40 (2.178)	42.43 (3.676)
STID	0.1791 (0.054)	74.17 (10.93)	11.47 (26.69)	0.1475 (0.043)	80.58 (9.611)	9.95 (26.25)	0.3429 (0.214)	51.25 (28.91)	-26.07 (78.68)
TSMixer	0.1322 (0.013)	83.19 (3.164)	34.65 (6.426)	0.1118 (0.013)	87.60 (3.217)	31.75 (7.936)	0.2258 (0.040)	65.32 (7.793)	16.99 (14.71)
Autoformer	0.2154 (0.052)	66.81 (9.184)	-6.48 (25.70)	0.1654 (0.031)	75.34 (5.968)	-0.98 (18.93)	0.4857 (0.199)	31.26 (24.42)	-78.57 (73.16)
Informer	0.1314 (0.001)	83.89 (0.270)	35.05 (0.494)	0.1062 (0.002)	89.61 (0.438)	35.16 (1.221)	0.1882 (0.018)	70.80 (5.120)	30.81 (6.618)
iTransformer	0.1230 (0.002)	85.61 (0.239)	39.20 (0.989)	0.1050 (0.003)	89.47 (0.599)	35.90 (1.832)	0.1585 (0.015)	78.34 (3.740)	41.73 (5.515)

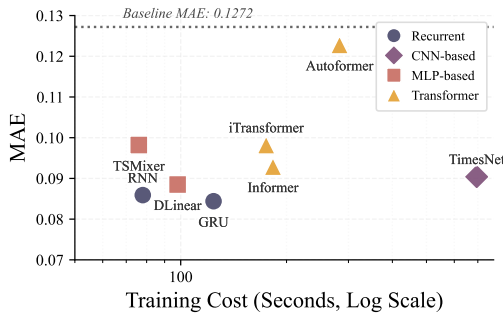


Figure 5: Efficiency-Accuracy Landscape (Solar S1, H=24). The scatter plot illustrates the trade-off between computational cost (Training Time per Epoch, Log Scale) and predictive performance (MAE). The dashed line represents the physical Baseline error (0.1272).

representing the optimal trade-off between speed and accuracy, is dominated by lightweight Recurrent (GRU, RNN) and MLP-based (DLinear, TSMixer) models. Notably, the GRU achieves the lowest

error ($MAE \approx 0.084$) while requiring nearly an order of magnitude less training cost than CNN-based alternatives. DLinear and TSMixer further demonstrate strong efficiency, training in under 100 seconds with competitive accuracy, making them well suited for resource-constrained deployment. In contrast, Transformer models (Informer, iTransformer, Autoformer) cluster in the upper-middle region, exhibiting a clear negative computational return. Despite incurring 2×–5× higher training costs than the GRU, they deliver inferior accuracy. The Autoformer is a notable outlier: its costly auto-correlation mechanisms fail to yield meaningful gains, achieving an $MAE \approx 0.122$ only marginally better than the naive Baseline. This indicates that the quadratic or log-linear complexity of attention mechanisms is poorly matched to renewable energy time series, where dynamics are primarily governed by local physical causality rather than long-range semantic dependencies. Overall, these findings suggest that, for operational renewable energy forecasting, *less is often more*, and that structurally aligned AR and MLP models offer a more compute-efficient path than increasingly over-parameterized architectures.

6 Conclusion

The introduction of R²Energy marks a paradigm shift in renewable energy forecasting, moving the focus from aggregate statistical precision toward operational robustness under diverse and extreme conditions. Our findings reveal a critical robustness-complexity trade-off, demonstrating that in safety-critical power systems, reliability is driven by the alignment between a model's inductive bias and physical causality rather than mere architectural complexity. By establishing a standardized, leakage-free protocol and introducing metrics, this work provides a principled foundation for evaluating whether AI models can withstand the high-impact, tail-risk events that threaten modern grid stability.

Moving forward, R²Energy serves as a catalyst for developing physically-augmented and climate-adaptive AI. It inspires a new generation of forecasting models that are not only computationally efficient but also capable of autonomously adapting their strategies when transitioning between stable regimes and high-entropy weather fronts. Ultimately, this benchmark bridges the gap between academic research and real-world deployment, guiding the development of trustworthy forecasting solutions essential for the global transition to a carbon-neutral energy future.

References

- [1] Stefano Alessandrini and Simone Sperati. 2017. Characterization of forecast errors and benchmarking of renewable energy forecasts. In *Renewable Energy Forecasting*. Elsevier, 235–256.
- [2] Sheraz Aslam, Herodotou, Syed Muhammad Mohsin, Nadeem Javaid, Nouman Ashraf, and Shahzad Aslam. 2021. A survey on deep learning methods for power load and renewable energy forecasting in smart microgrids. *Renewable and Sustainable Energy Reviews* 144 (2021), 110992.
- [3] Shaojie Bai. 2018. An Empirical Evaluation of Generic Convolutional and Recurrent Networks for Sequence Modeling. *arXiv preprint arXiv:1803.01271* (2018).
- [4] Robert Blaga, Andreea Sabadus, Nicoleta Stefu, Ciprian Dughir, Marius Paulescu, and Viorel Badescu. 2019. A current perspective on the accuracy of incoming solar energy forecasting. *Progress in energy and combustion science* 70 (2019), 119–144.
- [5] Oussama Boussif, Ghait Boukachab, Dan Assouline, Stefano Massaroli, Tianle Yuan, Loubna Benabbou, and Yoshua Bengio. 2023. Improving* day-ahead* solar irradiance time series forecasting by leveraging spatio-temporal context. *Advances in Neural Information Processing Systems* 36 (2023), 2342–2367.
- [6] Si-An Chen, Chun-Liang Li, Nate Yoder, Sercan O Arik, and Tomas Pfister. 2023. Tsmixer: An all-mlp architecture for time series forecasting. *arXiv preprint arXiv:2303.06053* (2023).
- [7] Junyoung Chung, Caglar Gulcehre, KyungHyun Cho, and Yoshua Bengio. 2014. Empirical evaluation of gated recurrent neural networks on sequence modeling. *arXiv preprint arXiv:1412.3555* (2014).
- [8] M Durgadevi et al. 2021. Generative Adversarial Network (GAN): A general review on different variants of GAN and applications. In *2021 6th International Conference on Communication and Electronics Systems (ICCES)*. IEEE, 1–8.
- [9] Jeffrey L Elman. 1990. Finding structure in time. *Cognitive science* 14, 2 (1990), 179–211.
- [10] Graeme Hawker, Keith Bell, Janusz Bialek, and Callum MacIver. 2024. Management of extreme weather impacts on electricity grids: an international review. *Progress in Energy* 6, 3 (2024), 032005.
- [11] Sepp Hochreiter and Jürgen Schmidhuber. 1997. Long short-term memory. *Neural computation* 9, 8 (1997), 1735–1780.
- [12] Yadong Lei, Zhili Wang, Deying Wang, Xiaoye Zhang, Huizheng Che, Xu Yue, Chenguang Tian, Junting Zhong, Lifeng Guo, Lei Li, et al. 2023. Co-benefits of carbon neutrality in enhancing and stabilizing solar and wind energy. *Nature Climate Change* 13, 7 (2023), 693–700.
- [13] Wenxiang Li and KL Eddie Law. 2024. Deep learning models for time series forecasting: A review. *IEEE Access* 12 (2024), 92306–92327.
- [14] Laibao Liu, Gang He, Mengxi Wu, Gang Liu, Haoran Zhang, Ying Chen, Jiashu Shen, and Shuangcheng Li. 2023. Climate change impacts on planned supply-demand match in global wind and solar energy systems. *Nature Energy* 8, 8 (2023), 870–880.
- [15] Laibao Liu, Yang Wang, Zheng Wang, Shuangcheng Li, Jiangtao Li, Gang He, Yan Li, Yanxu Liu, Shilong Piao, Ziqi Gao, et al. 2022. Potential contributions of wind and solar power to China's carbon neutrality. *Resources, Conservation and Recycling* 180 (2022), 106155.
- [16] Yong Liu, Tengge Hu, Haoran Zhang, Haixu Wu, Shiyu Wang, Lintao Ma, and Mingsheng Long. 2023. itransformer: Inverted transformers are effective for time series forecasting. *arXiv preprint arXiv:2310.06625* (2023).
- [17] Zhengjing Ma and Gang Mei. 2022. A hybrid attention-based deep learning approach for wind power prediction. *Applied Energy* 323 (2022), 119608.
- [18] Ziqing Ma, Wenwei Wang, Tian Zhou, Chao Chen, Bingqing Peng, Liang Sun, and Rong Jin. 2024. Fusionsf: Fuse heterogeneous modalities in a vector quantized framework for robust solar power forecasting. In *Proceedings of the 30th ACM SIGKDD Conference on Knowledge Discovery and Data Mining*. 5532–5543.
- [19] V Anantha Natarajan and Poojitha Karatampati. 2019. Survey on renewable energy forecasting using different techniques. In *2019 2nd international conference on power and embedded drive control (ICPEDC)*. IEEE, 349–354.
- [20] Joseph B Olson, Jaymes S Kenyon, Irina Djalalova, Laura Bianco, David D Turner, Yelena Pichugina, Aditya Choukulkar, Michael D Toy, John M Brown, Wayne M Angevine, et al. 2019. Improving wind energy forecasting through numerical weather prediction model development. *Bulletin of the American Meteorological Society* 100, 11 (2019), 2201–2220.
- [21] Franko Pandžić and Tomislav Capuder. 2023. Advances in short-term solar forecasting: A review and benchmark of machine learning methods and relevant data sources. *Energies* 17, 1 (2023), 97.
- [22] Athula TD Perera, Vahid M Nik, Deliang Chen, Jean-Louis Scarazzini, and Tianzhen Hong. 2020. Quantifying the impacts of climate change and extreme climate events on energy systems. *Nature Energy* 5, 2 (2020), 150–159.
- [23] Daniel Vázquez Pombo, Peder Bacher, Charalampos Ziras, Henrik W Bindner, Sergiu V Spataru, and Poul E Sørensen. 2022. Benchmarking physics-informed machine learning-based short term PV-power forecasting tools. *Energy Reports* 8 (2022), 6512–6520.
- [24] Mike Schuster and Kuldip K Paliwal. 1997. Bidirectional recurrent neural networks. *IEEE transactions on Signal Processing* 45, 11 (1997), 2673–2681.
- [25] Zehui Shao, Zhao Zhang, Fei Wang, Wei Wei, and Yongjun Xu. 2022. Spatial-temporal identity: A simple yet effective baseline for multivariate time series forecasting. In *Proceedings of the 31st ACM international conference on information & knowledge management*. 4454–4458.
- [26] Chunming Shen, Wei Zhu, and Liping Xu. 2020. Critical risk determination method of energy-flow network for urban electricity system under extreme heat wave impact. *Environmental Research* 191 (2020), 110143.
- [27] Jianjian Shen, Yue Wang, Mengke Lin, Chuntian Cheng, Jan K Kazak, Jian Wang, Xihai Guo, Xiufeng Li, Binbin Zhou, and Linsong Ge. 2025. Quantifying the impact of extreme weather on China's hydropower–wind–solar renewable energy system. *Nature Water* (2025), 1–15.
- [28] Alex Sherstinsky. 2020. Fundamentals of recurrent neural network (RNN) and long short-term memory (LSTM) network. *Physica D: Nonlinear Phenomena* 404 (2020), 132306.
- [29] Ajay Shrestha and Ausif Mahmood. 2019. Review of deep learning algorithms and architectures. *IEEE access* 7 (2019), 53040–53065.
- [30] Simone Sperati, Stefano Alessandrini, Pierre Pinson, and George Kariniotakis. 2015. The “weather intelligence for renewable energies” benchmarking exercise on short-term forecasting of wind and solar power generation. *Energies* 8, 9 (2015), 9594–9619.
- [31] Copernicus Climate Data Store et al. 2024. ERA5 hourly data on single levels from 1940 to present. *Datos recuperados entre noviembre* (2024).
- [32] Rita Teixeira, Adelaide Cerveira, Eduardo J Solteiro Pires, and José Baptista. 2024. Advancing renewable energy forecasting: A comprehensive review of renewable energy forecasting methods. *Energies* 17, 14 (2024), 3480.
- [33] Ashish Vaswani, Noam Shazeer, Niki Parmar, Jakob Uszkoreit, Llion Jones, Aidan N Gomez, Łukasz Kaiser, and Illia Polosukhin. 2017. Attention is all you need. *Advances in neural information processing systems* 30 (2017).
- [34] Guoyu Wang, Jiepeng Wu, and Jinsheng Zhou. 2025. Multi-objective Optimization Research on the Achievement Path of Dual Carbon Goals in Mining Enterprises. *Energy* (2025), 137194.
- [35] Huaizhi Wang, Zhenxing Lei, Xian Zhang, Bin Zhou, and Jianchun Peng. 2019. A review of deep learning for renewable energy forecasting. *Energy Conversion and Management* 198 (2019), 111799.
- [36] Haixu Wu, Tengge Hu, Yong Liu, Hang Zhou, Jianmin Wang, and Mingsheng Long. 2022. Timesnet: Temporal 2d-variation modeling for general time series analysis. *arXiv preprint arXiv:2210.02186* (2022).
- [37] Haixu Wu, Jiehui Xu, Jianmin Wang, and Mingsheng Long. 2021. Autoformer: Decomposition transformers with auto-correlation for long-term series forecasting. *Advances in neural information processing systems* 34 (2021), 22419–22430.
- [38] Luo Xu, Kairui Feng, Ning Lin, ATD Perera, H Vincent Poor, Le Xie, Chuanyi Ji, X Andy Sun, Qinglai Guo, and Mark O’Malley. 2024. Resilience of renewable power systems under climate risks. *Nature Reviews Electrical Engineering* 1, 1 (2024), 53–66.
- [39] Xin Xu, Qinglong Cao, Ruizhe Deng, Zhiling Guo, Yuntian Chen, and Jinyue Yan. 2025. A cross-dataset benchmark for neural network-based wind power forecasting. *Renewable Energy* (2025), 123463.

- [40] Mao Yang, Yunfeng Guo, and Yutong Huang. 2023. Wind power ultra-short-term prediction method based on NWP wind speed correction and double clustering division of transitional weather process. *Energy* 282 (2023), 128947.
- [41] Yiyuan Yang, Ming Jin, Haomin Wen, Chaoli Zhang, Yuxuan Liang, Lintao Ma, Yi Wang, Chenghai Liu, Bin Yang, Zenglin Xu, et al. 2024. A survey on diffusion models for time series and spatio-temporal data. *Comput. Surveys* (2024).
- [42] Xi Yuan, Chi-Wei Su, Muhammad Umar, Xuefeng Shao, and Oana-Ramona Lobon. 2022. The race to zero emissions: Can renewable energy be the path to carbon neutrality? *Journal of Environmental Management* 308 (2022), 114648.
- [43] Ailing Zeng, Muxi Chen, Lei Zhang, and Qiang Xu. 2023. Are transformers effective for time series forecasting?. In *Proceedings of the AAAI conference on artificial intelligence*, Vol. 37. 11121–11128.
- [44] Jin Zhao, Fangxing Li, and Qiwei Zhang. 2024. Impacts of renewable energy resources on the weather vulnerability of power systems. *Nature Energy* 9, 11 (2024), 1407–1414.
- [45] Dongsheng Zheng, Dan Tong, Steven J Davis, Yue Qin, Yang Liu, Ruochong Xu, Jin Yang, Xizhe Yan, Guannan Geng, Huizheng Che, et al. 2024. Climate change impacts on the extreme power shortage events of wind-solar supply systems worldwide during 1980–2022. *Nature Communications* 15, 1 (2024), 5225.
- [46] Dongsheng Zheng, Xizhe Yan, Dan Tong, Steven J Davis, Ken Caldeira, Yuanyuan Lin, Yaqin Guo, Jingyun Li, Peng Wang, Liying Ping, et al. 2025. Strategies for climate-resilient global wind and solar power systems. *Nature* (2025), 1–3.
- [47] Haoyi Zhou, Shanghang Zhang, Jieqi Peng, Shuai Zhang, Jianxin Li, Hui Xiong, and Wancai Zhang. 2021. Informer: Beyond efficient transformer for long sequence time-series forecasting. In *Proceedings of the AAAI conference on artificial intelligence*, Vol. 35. 11106–11115.
- [48] Xiangrong Zhu, Junhao Tian, and Yu Wang. [n. d.]. The Impact of Climate Change on Wind and Solar Photovoltaic Power Potential and Distribution in China. *Available at SSRN 4986631* ([n. d.]).
- [49] Yiping Zhu, Yang Hu, and Yi Zhu. 2024. Can China's energy policies achieve the "dual carbon" goal? A multi-dimensional analysis based on policy text tools. *Environment, Development and Sustainability* (2024), 1–40.

Received 20 February 2007; revised 12 March 2009; accepted 5 June 2009